Journal of Alloys and Compounds 789 (2019) 588–594

Contents lists available at ScienceDirect

Journal of Alloys and Compounds

journal homepage: http://www.elsevier.com/locate/jalcom

Investigation of the high pressure phase BiS_2: Temperature-resolved structure and compression behavior to 60 GPa

Simone M. Kevy [a], Morten B. Nielsen [a], Lars F. Lundegaard [b], Davide Ceresoli [c], Yu-Sheng Chen [d], Hazel Reardon [a], Paraskevas Parisiades [e, f], Martin Bremholm [a, *]

[a] Center for Materials Crystallography (CMC), Department of Chemistry and iNANO, Aarhus University, Langelandsgade 140, 8000, Aarhus C, Denmark
[b] Haldor Topsoe, Nymøllevej 55, 2800, Kgs. Lyngby, Denmark
[c] Center for Materials Crystallography and Institute of Molecular Science and Technology (CNR-ISTM), Via Golgi 19, 20133, Milano, Italy
[d] ChemMatCARS, The University of Chicago, Advanced Photon Source, Argonne, IL 60439, USA
[e] ID27 Beamline, European Synchrotron Radiation Facility, 71 Avenue des Martyrs, 38043 Grenoble, France
[f] Institut de Minéralogie de Physique des Matériaux et de Cosmichimie, 4 Place Jussieu, F-75005, Paris, France

ARTICLE INFO

Article history:
Received 7 September 2018
Received in revised form
28 February 2019
Accepted 2 March 2019
Available online 5 March 2019

Keywords:
BiS_2
Chalcogenides high-pressure
Superconductors
Heat capacity

ABSTRACT

BiS_2 was synthesized using a multi-anvil large volume press at a pressure and temperatures of 5.5 GPa and 1250 °C, respectively, and was then recovered at ambient conditions. Using data collection from single crystal synchrotron X-ray diffraction experiments, the crystal structure was found to consist of two distinct distorted square-based pyramidal BiS_5-units. Synchrotron powder X-ray diffraction in the 85–300 K range shows smooth thermal expansion with a modest anisotropy. Physical property measurements reveals an optical band gap of 1.10 eV and a heat capacity with no anomalies in the 2–300 K range. Debye temperatures, determined by both heat capacity and thermal motion analysis, agree well with values of around 114 and 107 K for Bi1 and Bi2 atoms, respectively. Furthermore, theoretical calculations of the electronic band structure, by density functional theory, confirm the gapped state and reveal a small degree of band inversion at the Γ-point, but calculation of parity eigenvalues show BiS_2 to possess a trivial topology. The high pressure behavior up to 60 GPa was investigated by powder diffraction in a diamond anvil cell; the structure is retained to at least 35 GPa while indications of a structure transition are observed afterwards. Fitting a 3rd order Birch-Murnaghan equation of state for pressures up to 30 GPa gives a bulk modulus of $K_0 = 35.5(8)$ GPa and $K_0' = 7.37(18)$. Finally, a short structural comparison between the high pressure phase of BiS_2 and BiS_2-based superconductors is presented.

1. Introduction

High pressure synthesis is an important method in the search for new compounds, where long-lived metastable phases can be recovered at ambient conditions. The system under investigation belongs to the metal dichalcogenides, MX_2 (X = S, Se, Te). These compounds have been studied extensively incorporating transition metals [1]. The high interest in these compounds arises from their unique crystal structures and electrical properties [2,3]. They crystallize in either 2D or 3D structures, depending on the result of the interaction between cationic *d*-levels and anionic *sp*-levels [4]. The layered MX_2 structures consist of X-*M*-X layers held together by van der Waals forces. Both Sn and Pb (group 14) form sulfide compounds which are stable at ambient pressure. Pyrite-type PbS_2 is a stable compound formed at ambient pressure, while $PbSe_2$ requires pressure and heating to form. $PbSe_2$ crystallizes in the $CuAl_2$ type structure consisting of alternating layers of Pb and Se, where Se exists as $[Se_2]^{2-}$ dimers with the Pb^{2+} in square antiprismatic coordination with Se [5]. For the group 15 elements that form chalcogenides, the highest metal to chalcogenide ratio in the phase diagram is 2:3. For the Bi–S phase diagram, the most sulfur-rich phase is Bi_2S_3 (bismuthinite), belonging to the tetradymite-type structure [6,7]. The more S-rich compound, BiS_2, was discovered by high pressure and high temperature synthesis and was reported as early as the 1960's, but no structure solution was reported at that time [8].

Recent discoveries of BiS_2-based superconductors, i.e. Ln(O,F)BiX_2 (X = S, Se; Ln = La, Ce, Nd) and $Bi_4O_4S_3$, adds further

* Corresponding author.
E-mail address: bremholm@chem.au.dk (M. Bremholm).

https://doi.org/10.1016/j.jallcom.2019.03.023
0925-8388/

motivation and renewed interest in the bulk BiS_2 compound [9–14]. The structure of Ln(O,F)BiS_2 contains Ln(O,F) blocking layers which donate electrons to the superconducting BiS_2 layer. The BiS_2 layers have a rock-salt structure with Bi and S atoms aligned alternately on a square lattice. The O/F ratio can be used to tune the T_C, the highest reported value being 10.6 K for La(O,F)BiS_2 [15]. The La(O,F)BiS_2 compound has also been studied for its thermoelectric properties, motivated by its resemblance to layered bismuth chalcogenides such as Bi_2Te_3 [16].

Here, we report the high pressure synthesis and behavior of BiS_2 together with the thermal expansion from 85 to 300 K. Quenching during the synthesis is shown to be essential to obtain phase pure samples. The structure was solved with single crystal synchrotron X-ray diffraction data. The structures of BiS_2 and the structurally similar $BiSe_2$ were previously solved by Yamamoto et al. [17] and we compare their reported synthesis and structural parameters with those determined independently for BiS_2 in this work. Measurements of heat capacity and the optical band gap are discussed in relation to calculations of the electronic band structures for BiS_2 and $BiSe_2$ and the possibilities of non-trivial topological surface states and pressure-induced superconductivity (as found in e.g. Bi_2Te_3) are also discussed [18].

2. Methods

Fine powders of the pure elements, bismuth (99.999%) and sulfur (99.999%), were mixed in a molar ratio of 1:3, i.e. a large excess of sulfur. Phase pure samples of bismuth disulfide, BiS_2, were then synthesized using high pressure and high temperature in a multi-anvil large volume press (MaVo LP 1000-540/50) equipped with a Walker-type module (MaVo). 14/8 octahedral assemblies from COMPRES were used with a MgO sample container [19] together with type C thermocouples positioned close to the sample. Pressure calibration was done by following polymorphic transitions in bismuth at room temperature and was found to be in good agreement with *in-situ* results obtained on the same type of octahedra [19,20].

Heating rates of 75 °C/min and hold times of 5–10 min were employed, followed by turning off the furnace power thereby quenching the sample to room temperature. Different temperatures in the range of 1200–1375 °C were investigated either with immediate quenching or ramped cooling before quenching. Single crystal growth was carried out during compressions by slow cooling (with rates of 2 and 5 °C/min) from temperatures of 1200 °C down to 800 °C, before quenching. Residual sulfur in the products was dissolved in CS_2.

Single crystal X-ray diffraction was measured at a temperature of 100(1) K at the Advanced Photon Source (APS) synchrotron, ChemMatCARS beamline ID-15-B ($\lambda = 0.41328$ Å) using a Bruker D8 diffractometer with an APEXII CCD detector. For PXRD, a powdered BiS_2 sample was loaded in a 0.1 mm quartz capillary and data was measured in transmission geometry at the SPring-8 synchrotron on BL44B2, for seven different temperatures from 85 to 300 K obtained by a nitrogen gas cryojet [21]. Rietveld refinements were performed using FullProf [22].

High pressure PXRD was performed from ambient pressure to 60 GPa using a membrane diamond anvil cell (DAC) with helium as pressure medium in a rhenium gasket. The experiment was performed at the European Radiation Synchrotron Facility (ERSF) in Grenoble, beamline ID27 [23]. The pressure was determined using the equation of state (EoS) for Au which was loaded in the DAC [24]. Extraction of the unit cell parameters from the 2D high pressure data was performed by refinements in the MAUD program [25–27] using the arbitrary texture model which is the 2D equivalent of a Le Bail refinement. EoS models for BiS_2 were fitted using the EosFit7c program [28].

Heat capacity was measured with a Quantum Design Physical Property Measurement System (QD-PPMS) on a thin disc of compressed powder of BiS_2. The addenda data was measured with the Apiezon N vacuum grease used to fixate the thin disc of BiS_2.

DFT calculations were performed within the plane-wave pseudopotential framework using the Quantum-Espresso package [29]. Fully relativistic norm-conserving [30] pseudopotentials were generated for Bi, S and Se. A detailed description of the calculations are provided in the Supplementary Information (SI).

3. Results and discussion

The high pressure synthesis of a compound with the composition BiS_2 was first reported by Silverman in 1964 [8], but our first attempts at reproducing the synthesis yielded samples with significant amounts of Bi_2S_3. In our study, we found that quenching to room temperature after heating was essential for producing phase pure samples. The optimal conditions for phase pure powder samples of BiS_2 were found to be a pressure of 5.5 GPa, holding at a temperature of 1250 °C for 5 min followed by quenching to RT.

Single crystals with rod-like dimensions of the order of $30 \times 100\ \mu m^2$ and a thickness of a few microns were grown by slow cooling (2 °C/min) from 1200 to 800 °C at 5.5 GPa followed by quenching to RT. Experiments applying cooling rates of 5 °C/min, as reported by Yamamoto et al., did not result in any single crystals of significant size, and the products contained a large proportion of Bi_2S_3.

The unit cell of BiS_2 is illustrated in Fig. 1a where the bismuth atom is confined to two different atomic sites. Both Bi atoms are coordinated to five S atoms in a distorted square-based pyramidal arrangement. The distortion comes from the fact that the bismuth atom is positioned slightly below the basal plane of the pyramid. The sulfur atoms surrounding the central bismuth atom can be divided into two groups: One that is shared between three edge-sharing neighboring polyhedra (Fig. 1c) called S2 for Bi1 (S3 for Bi2), and one that is in the outer position of the polygon row, shared only between two of the adjacent polyhedra. The last group (S1 for Bi1, S4 for Bi2) forms disulfide bonds to other S1 (S4) atoms in parallel neighboring rows.

The disulfide bonds are all parallel to each other and perpendicular to the *b*-axis, giving a ladder-like structure between the polyhedron rows, see Fig. 1a. A comparison of the bonding information and polyhedron volumes for the two different polyhedra are collated in supporting information (SI) Table S1.

The difference in bonds lengths in the basal plane of the Bi1–S1 and Bi1–S2 polyhedra is 0.136(3) Å, while the difference between Bi2–S3 and Bi2–S4 is significantly smaller, only 0.030(4) Å. This results in an off-centering of the Bi1 atoms which are slightly displaced towards the inner S2 atoms and away from the S1 involved in disulfide bonds (see Fig. 1b). This may be explained by the way the bismuth atom is coordinated to its neighbors. The Bi2 atom is facing the center of a triangular face of three sulfur atoms of the opposite Bi1 polyhedra, as shown by arrows in Fig. 1a. The Bi1 atom is on the other hand directed towards an edge of the pyramid shared between only two sulfur atoms. Thus, this could be the explanation of the difference in the off-centering of the middle bismuth atom. Concerning the lone pair on the bismuth atom, it is possible that it is located in the empty channels between the rows of polyhedra since the interlayer distance in the structure is only 1.7 Å, which is much shorter than typical van der Waals bonds. The S1–S1 and S4–S4 dimer bond lengths are 2.053(6) and 2.093(5) Å, respectively. Bond valence sums give S1–S1 and S4–S4 valences of 0.916 and 1.019, respectively, and they can therefore be considered as fully oxidized $[S_2]^{2-}$ dimers. This is comparable to the dimer

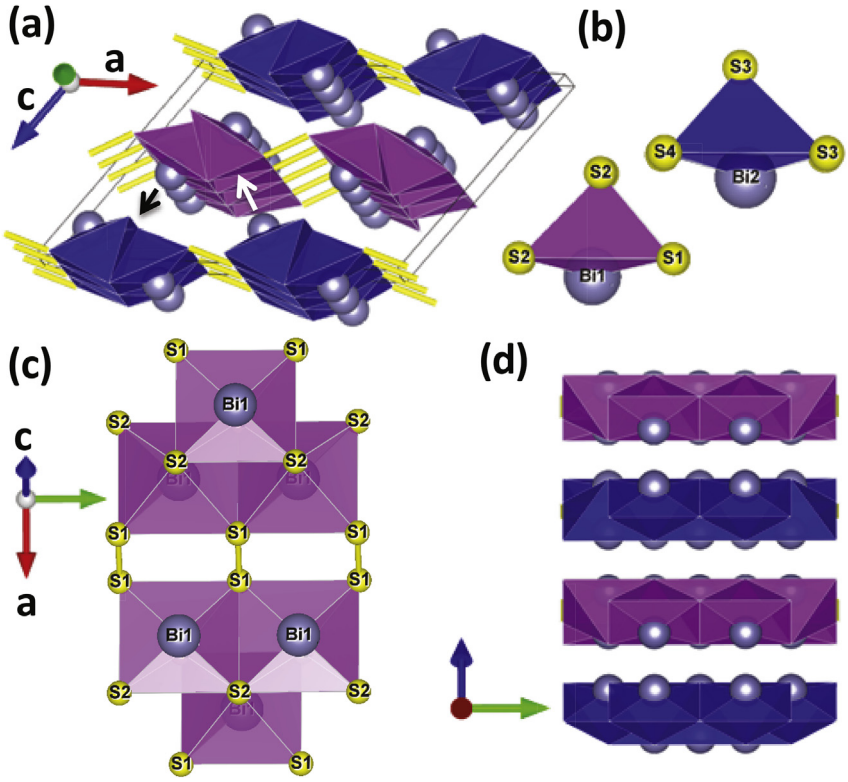

Fig. 1. (a) The unit cell of BiS_2; Bi atoms (grey) are positioned in polyhedra (purple (Bi1) or blue (Bi2)) with S atoms (yellow when shown in polyhedra) in each corner, and S-S bonds are marked in yellow. The black arrow indicates the coordination of the Bi1 with the neighboring polyhedron, which is facing an edge with two S atoms. The white arrow indicates the coordination of the Bi2 atom which is oriented towards a face of the opposite polyhedron shared between three sulfur atoms. (b) The two bismuth polyhedral and the dedicated sulfur atoms. Bi1 is surrounded by S1 and S2, and Bi2 by S3 and S4. (c) Focus on the disulfide bonds showing corner linkage of different bismuth polyhedra. (d) Expanded structure representation showing layered polyhedra connected along the *b*-direction. (For interpretation of the references to colour in this figure legend, the reader is referred to the Web version of this article.)

distances found by Yamamoto et al. (2.047(4) Å and 2.082(3)), but they do not comment on the difference between the two dimer lengths.

3.1. Rietveld refinements

Rietveld refinements of seven temperature-resolved BiS_2 PXRD data sets (85–300 K) show single-phase diffraction patterns in good agreement with the structural parameters obtained from SC-XRD, as illustrated by the 300 K refinement in Fig. 2a. The obtained unit cell axis lengths and volume display a linear expansion (Fig. 2b), while the monoclinic angle, β, shows a subtle linear decrease with increasing temperature. The thermal expansion coefficients are: $\alpha_a = 7.1(2) \cdot 10^{-6}\,K^{-1}$, $\alpha_b = 1.86(2) \cdot 10^{-5}\,K^{-1}$, $\alpha_c = 1.57(2) \cdot 10^{-5}\,K^{-1}$ and $\alpha_V = 4.47(6) \cdot 10^{-5}\,K^{-1}$. The thermal expansion along the *a*-axis is less than half of the expansion along the *b*- and *c*-axes. The S—S dimer bonds extend along the *a*-axis and connect the polyhedral columns, and the more rigid nature of the bonding in the sulfur dimers is responsible for the anisotropy of the thermal expansion.

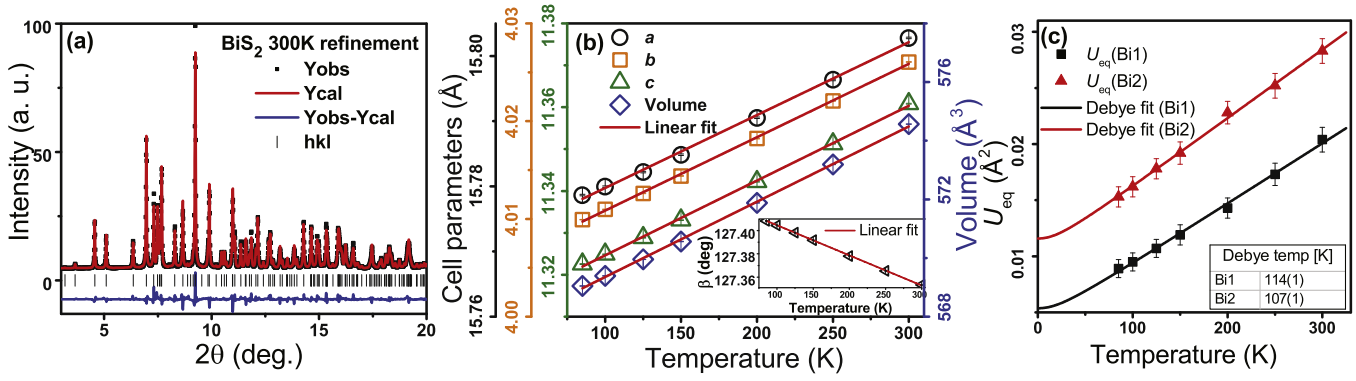

Fig. 2. (a) Rietveld refinement of BiS_2 at 300 K, where the observed data are represented as black points, the calculated model as the red line, the difference curve by the blue line, and *hkl* reflections are indicated as black tick marks. (b) Cell parameters and volume as a function of temperature for BiS_2. The inset shows the β angle. (c) U_{eq} as a function of temperature for the two Bi atoms in BiS_2. Solid lines represent the fit of the full Debye model, and the legend displays the resulting Debye temperatures from the linear expression. (For interpretation of the references to colour in this figure legend, the reader is referred to the Web version of this article.)

The absence of structural transitions indicated by the smooth thermal expansions are also reflected in the atomic structure of BiS_2 and the thermal parameters. Geometric analysis shows that the bond lengths for Bi–S bonds in the pyramids shows decreases down to 85 K (Fig S5 in SI). The anisotropy is observed for the pyramid volumes and the S–S dimer bond lengths (Fig S4 in SI). From the anisotropic thermal parameters of the two Bi atoms, the equivalent isotropic displacement parameter U_{eq} was fitted with a Debye model to extract the Debye temperature, Θ_D [31]. Fig. 2c displays the Debye fit to the thermal parameters of the Bi atoms and the Debye temperatures determined from the two different models, 114(3) K for Bi1 and 107(2) K for Bi2. These values can be compared to the Debye temperature obtained from a heat capacity measurement performed in this study. The measurement showed Debye-behavior with a value of 80 J $K^{-1}mol^{-1}$ at room temperature and zero at 2 K, and no anomalies were observed (Fig. S7.a in SI). With the Debye model, a linear fit of C_v/T vs T^2 confirms the gapped state and is in agreement with the analysis of the UV–Vis spectra, which concluded BiS_2 to be a semiconductor with a band gap of 1.10 eV (Fig. S7b and c). Using the low temperature approximation of the Debye model, the Debye temperature (Θ_D) is found to be 114.2(2) K. This is in good agreement with the Debye temperatures obtained from thermal parameters obtained from the Rietveld refinements. The heat capacity measurement includes contributions from all atoms, and the good agreement shows that Bi atoms are the main contributor, and close to that of elemental bismuth of 116 K [32].

3.2. High pressure powder X-ray diffraction

Selected PXRD patterns of BiS_2 from ambient pressure to 60 GPa are shown in Fig. 3a. The most intense reflection (traced by the black dotted line in Fig. 3a and $2\theta = 7°$ at ambient pressure) follows a smooth increase to higher angles, as expected for a uniform compression. The reflections become broader with the increasing pressure, and the main reflection (at 6.9°) has almost disappeared in the pattern at the highest pressure, indicating either a phase transition or pressure-induced texture due to high strain. Between 39 and 45 GPa (Fig. 3b) peak splitting and intensity shifts are observed for reflections of the main peak, but this can be explained by multiple *hkl*-values (that overlap at ambient conditions) that spreads out at higher pressures. While the detailed atomic structural changes are not obtainable from the data, analysis of the unit cell parameters up to 30 GPa offers some insight.

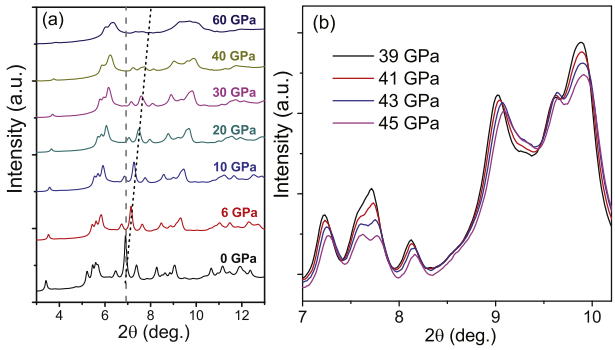

Fig. 3. DAC powder diffraction data for BiS_2 from ambient pressure to 60 GPa. (a) Overview of the PXRD data, with the vertical grey line indicating the strongest peak position (at 6.9°) for the ambient pressure pattern and a black dotted line following the shifting of the peak. (b) Zoom in on the peaks at 2θ: 7–10.5° for pressures between 39 and 45 GPa.

3.3. Refinement and equation of state

Due to significant peak broadening for pressures above 30 GPa the results from the refinement of our model against the data are interpreted with caution. The increase in the *c*-axis starting at approx. 35 GPa together with the unphysical increase of the unit cell volume at higher pressures indicates that the refined structure model is not representative of the data above 35 GPa and suggests that a phase transition to a lower symmetry has occurred. Our structure analysis of BiS_2 therefore focuses on the refinement for pressures up to 30 GPa.

The unit cell volume was fitted to several equation of state (EoS) models for pressures up to 30 GPa, and the zero pressure values of the volume (V_0), bulk modulus (K_0), and derivatives of the bulk modulus (K_0' and K_0'') obtained from all EoS fits can be found in SI in Table S5. The 3rd order Birch-Murnaghan (BM3) EoS provides the best fit and is included as a solid line in Fig. 4 which displays the normalized unit cell parameters and cell volume of BiS_2 with increasing pressures. The fit parameters obtained for the BM3 EoS are: $V_0 = 572.4(6)$ Å^3, $K_0 = 35.5(8)$ GPa and a rather high $K'_0 = 7.37(18)$ but often observed for 2D-like structures. The axial compression from ambient pressure to 30 GPa is largest for the *c*-axis which is reduced by 12%, while the *b*-axis is reduced by 10% and finally the *a*-axis by only 7%. See Table S6 and S7 in the SI for details about the axial and bulk EoS fitting. The monoclinic angle β remains almost constant up to the 30 GPa. In combination, this results in a reduction of the unit cell volume by 26% at 30 GPa as shown in Fig. 4a. Compared to Bi_2S_3, with a bulk modulus of $K_0 = 38.9(8)$ GPa and $K'_0 = 5.5(1)$ [33,34], BiS_2 is initially slightly more compressible but with the larger derivative it becomes less compressible than Bi_2S_3 at elevated pressure.

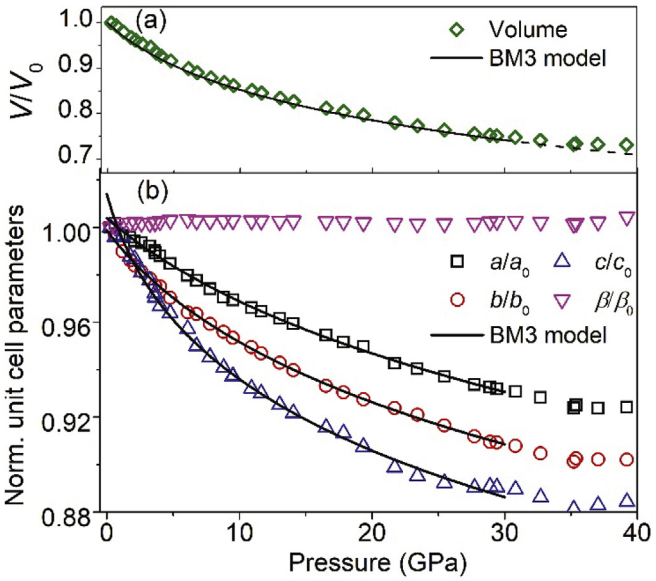

Fig. 4. Pressure dependence for (a) the normalized volume and (b) unit cell parameters of BiS_2 up to 40 GPa. The pressure evolution for BiS_2 is fitted with a 3rd order Birch-Murnaghan EoS (up to 30 GPa) for all. The line has been extrapolated to higher pressures for the volume to emphasize the expected behavior if no changes in the compressibility took place (red dashed line) at higher pressures. Error bars are smaller than the symbols and are therefore omitted for clarity. (For interpretation of the references to colour in this figure legend, the reader is referred to the Web version of this article.)

3.4. Theoretical calculations

Theoretical calculations were performed for BiS_2 and $BiSe_2$, but here we limit the discussion to BiS_2 and refer to the SI for further details and the results for $BiSe_2$. A full structural relaxation of both ionic degrees of freedom and lattice parameters was performed for BiS_2 starting from the structure determined by single crystal diffraction at 100 K. The calculated equilibrium cell volume at 0 K is 0.4% smaller than the experimental value. This contraction is also reflected in the bond lengths which are within 0.1–0.7% of the experimental values. Taking the temperature difference into account, there is an excellent agreement between the experimental and the calculated interatomic distances.

Band inversion as a result of spin orbit interaction (SOI) is one of the criteria for a non-trivial topology of the band structure. Fig. 5 shows the calculated band structure of BiS_2 and the density of states (DOS) with atomic orbital projections. The calculations at the GGA-PBE level show that BiS_2 is a direct-band gap semiconductor with a band gap of 0.64 eV. The optical band gap calculated from UV–Vis–NIR spectra showed a larger value of 1.10 eV (See SI, section 7 for details). This difference is typical for GGA-PBE functionals, which are known to underestimate band gaps by 40–60% [35].

By comparing the band structures calculated with and without SOI (see SI, Figs. S9–S10), we note that valence band of BiS_2 is nearly unchanged by addition of the SOI, and only small changes occur in the conduction bands. In the absence of SOI, the band gap increases to 1.07 eV and the gap becomes indirect. Regarding the possibility of a topological insulating state, we concentrate on the heaviest ion. The Bi ion is found to contribute to the top of the valence band. In Fig. 6 we highlight the Bi and S character of the band near the Fermi level. The splitting and the shape of the SOI bands at the bands edges does not show changes of convexity (i.e. s -> p inversion). Similarly to what is reported in Ref. [17], the amount of Bi orbitals at the top of the valence band, is too small for a topological state. For a quantitative estimate of band inversion one should calculate the "spin orbit spillage" as shown in Ref. [36]. However, since the system is inversion-symmetric, we calculated the Z_2 topological index as the product of the parity eigenvalues [37] at the eight Time Reversal Invariant Momenta (TRIM). For both BiS_2 and $BiSe_2$ the sums of the eigenvalues are zero and they are therefore trivial insulators by DFT (detailed results in Table S8 in SI).

3.5. Structural comparison of BiS_2 with BiS_2-based superconductors

From our analysis of high pressure BiS_2, the compound is found to be a trivial insulator with an optical band gap of 1.10 eV. This is in sharp contrast to the layered BiS_2-based superconductors with superconductivity arising from the BiS_2 layer. The parent compound of these systems is found to be a band insulator but, with electron doping, the resulting compounds become metallic and exhibit superconductivity [13,15]. Therefore, it seems that enhanced electron doping would be essential if the bulk BiS_2 high pressure compound should show the same trend.

A structural comparison of the high pressure phase of BiS_2 (Fig. 7a) with the BiS_2 layers of the $LaO_{0.5}F_{0.5}BiS_2$ superconductor (Fig. 7b) could improve understanding of the large difference in the physical properties. The BiS_2 layers in the superconductor have a rock salt-type structure with the *P*4/*nmm* space group, and each layer consists of two rows of BiS_2-layers.

The two compounds are compared by overlaying their structures in the dashed square indicated in Fig. 7.c. In both structures the bismuth atoms are coordinated to five sulfur atoms: $LaO_{0.5}F_{0.5}BiS_2$ form almost ideal square-based pyramids (S1–Bi1–S1 angle of 178.2(2)°) while these are highly distorted in the HP phase (161.4(2)° for the S1–Bi1–S2 angle). In HP BiS_2, the bismuth atom is displaced further out of the basal plane of the pyramid, i.e. the S1 and S2 atoms are slightly shifted up towards the apical S2. This inevitably pushes the apical S2 further away from Bi1, and therefore the bond length is longer (2.610(5) Å) compared to that of the SC phase Bi1–S2 distance (2.535(6) Å). In the SC phase, the BiS_2 layers consist of two chains of Bi1–S1–Bi1–S2 in the *b*-direction and the polyhedra on one chain are all positioned the same way. In the HP phase, the chains propagate along the a-axis, where the disulfide bonds connect the polyhedra in the opposite direction (relative to the HP phase). Both phases have a layered-type structural arrangement, but the gap between the layers in the HP phase is much smaller (1.7 Å), than the van der

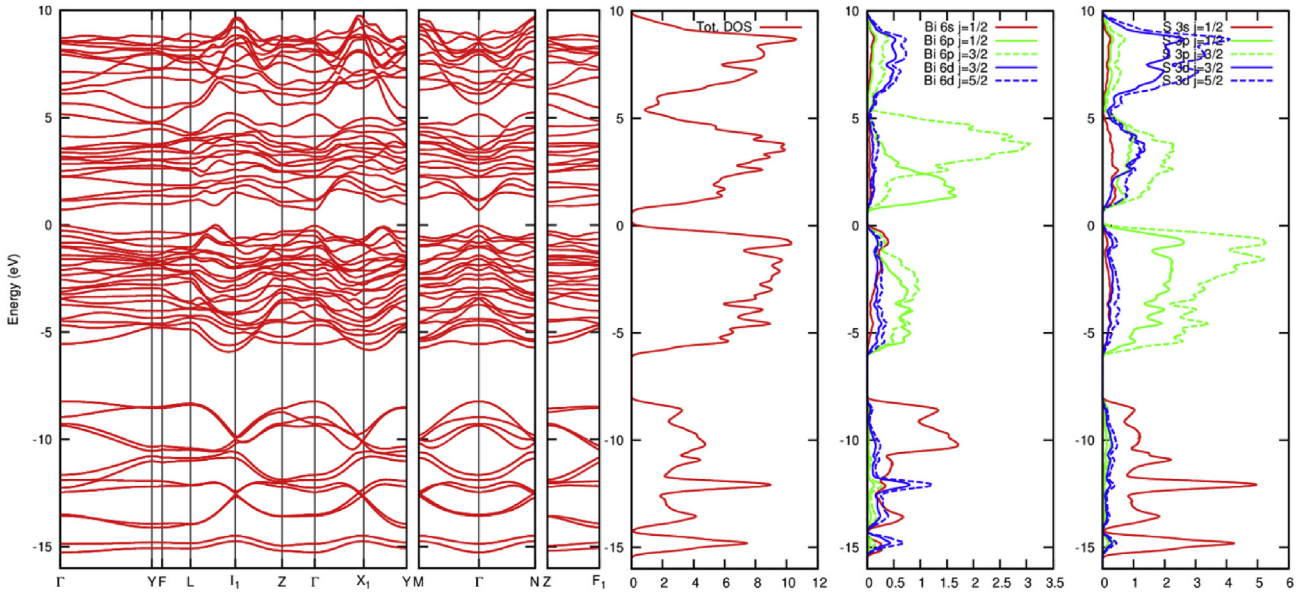

Fig. 5. Calculated BiS_2 band structure, including spin-orbit interaction. The zero energy is aligned with the top of the valence band. The Brillion zone of BiS_2 is shown in SI in Fig. S11. Calculated density of states for BiS_2 (number of states per eV), both the total and projected. The top of the valence band is at 0 eV.

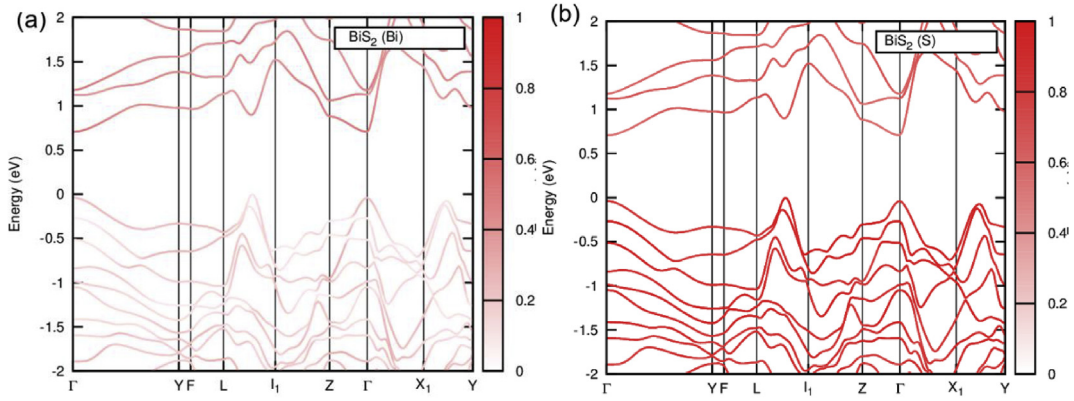

Fig. 6. Projected band structures of BiS_2. The intensity of the lines is proportional to the projection on the atomic orbitals of the ion. (a) Projection on Bi orbitals. (b) Projection on S orbitals. Note the very small contribution of Bi to the top of the valence band.

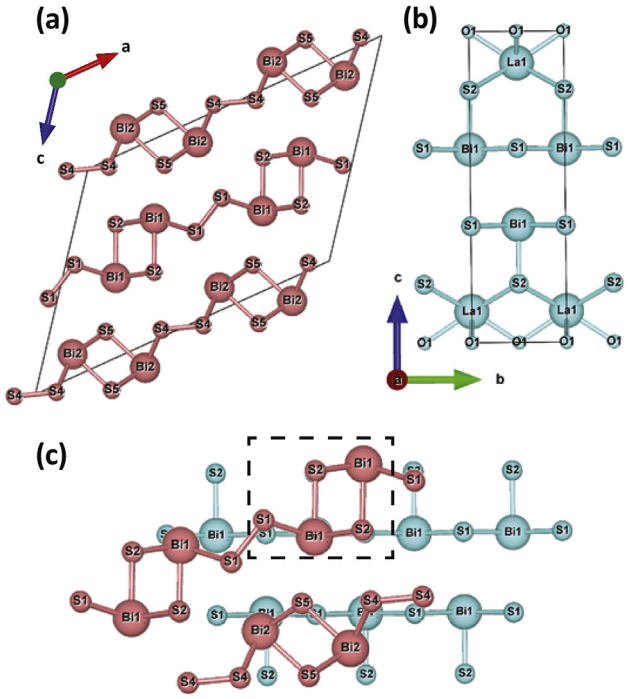

Fig. 7. (a) The high pressure phase of BiS_2. (b) The BiS_2-based superconductor of $LaO_{0.5}F_{0.5}BiS_2$. (c) Comparison of the high pressure phase of BiS_2 (red) with the BiS_2-layers from the $LaO_{0.5}F_{0.5}BiS_2$ superconductor (blue). The dashed square in the figure is to highlight the area in the structure where the two structures have a similar arrangement. (For interpretation of the references to colour in this figure legend, the reader is referred to the Web version of this article.)

Waals gap of 3.2 Å in the SC BiS_2 layers. The compacted high pressure phase is therefore significantly different from the superconducting BiS_2 layers.

4. Conclusions

BiS_2 was synthesized at 5.5 GPa and 1250 °C using a large volume press equipped with a walker module. Quenching from the set point temperature to room temperature was demonstrated to be crucial for obtaining phase pure samples. Single crystals were obtained after slow cooling from 1200 to 800 °C followed by temperature quenching. The structural solution by micro-focused synchrotron single crystal X-ray diffraction confirmed that BiS_2 crystallizes in a monoclinic structure with space group *C*2/*m*. The structure consists of distorted square-based pyramidal BiS_5 polyhedra connected to the neighboring polyhedra through S atoms that form chains along the *b*-axis. These chains are connected by disulfide bonding such that every fourth S atom is part of an S–S dimer. A comparison of the BiS_2-based superconductors with the high pressure phase of BiS_2 were presented. The difference in bond lengths and coordination underlines how the pyramidal arrangement of the bismuth atoms in the high pressure BiS_2 structure are more distorted than in the superconductor. Refinements of the crystal structure against data in the temperature range from 300 to 85 K indicated that no drastic change occurs in the structure of BiS_2. The ambient-pressure structure of BiS_2 is compressed without detecting any structural changes down to 35 GPa; beyond that pressure, the PXRD patterns display very strong broadening of the peak profiles, and a detailed structural analysis could not be justified.

BiS_2 is a semiconductor with an optical band gap of 1.10 eV as determined by UV–Vis–NIR spectroscopy. Measurement of heat capacity showed no anomalies from 2 to 300 K, and revealed the behavior to be as expected for a semiconductor. The Debye temperature of 114.2(2) K, calculated from the heat capacity, was found to be in good agreement with the Debye temperatures calculated from the thermal motion analysis of 114(3) K and 107(2) K for Bi1 and Bi2, respectively. Calculations of the electronic band structure by DFT confirmed a gapped state and the compound is found to have trivial topology.

The high structural integrity of BiS_2 up to 35 GPa adds to the question of when the band gap closes and whether the compound could become superconducting at high pressure in analogy to the behavior of the topological insulator Bi_2Te_3. The structural robustness allows introduction of electron donating dopants, as is also required in the superconductor La(O,F)BiS_2, where the electrons are donated from the blocking layers to the superconducting BiS_2 layers. Furthermore, the band gap could be closed at high pressure and could result in a superconducting state.

Acknowledgements

MB thanks the Villum Foundation (VKR022450) and CMC for funding. CMC is a Center of Excellence funded by the Danish National Research Foundation (DNRF93). The Danish Agency for Science, Technology and Innovation (DANSCATT) is acknowledged for supporting the synchrotron activities. We thank the RIKEN SPring-8 center for beam time at beamline BL44B2 (RIKEN proposal no. 20150018), ESRF for beamtime on ID27 and the Advanced Photon

Source for beamtime on ChemMatCARS, ID15B. ChemMatCARS is principally supported by the Divisions of Chemistry (CHE) and Materials Research (DMR), National Science Foundation, under grant number NSF/CHE-1834750. Use of the APS, an Office of Science User Facility operated for the US Department of Energy (DOE) Office of Science by Argonne National Laboratory, was supported by the US DOE under Contract No. DE-AC02-06CH11357.

Appendix A. Supplementary data

Supplementary data related to this article can be found at https://doi.org/10.1016/j.jallcom.2019.03.023.

References

[1] L. Merrill, Behavior of the AB_2 type compounds at high pressure and high temperatures, J. Phys. Chem. Ref. Data 11 (4) (1982) 1005. https://doi.org/10.1063/1.555670.
[2] M. Chhowalla, H.S. Shin, G. Eda, L.-J. Li, K.P. Loh, H. Zhang, The chemistry of two-dimensional layered transition metal dichalcogenide nanosheets, Nat. Chem. 5 (2013) 263–275. https://doi.org/10.1038/NCHEM.1589.
[3] E. Selvi, R. Aksoy, R. Knudson, Y.Z. Ma, High-pressure X-ray diffraction study of tungsten diselenide, J. Phys. Chem. Solids 69 (2008) 2311–2314. https://doi.org/10.1016/j.jpcs.2008.04.003.
[4] M. Bouroushian, Electrochemistry of Metal Chalcogenides, first ed., Springer, 2010.
[5] M. Bremholm, Y.S. Hor, R.J. Cava, Pressure stabilized Se-Se dimer formation in $PbSe_2$, Solid State Sci. 13 (2011) 38–41. https://doi.org/0.1016/j.solidstatesciences.2010.10.003.
[6] J.-C. Lin, R.C. Sharma, Y.A. Chang, The Bi-S (bismuth-sulfur) system, J. Phase Equilibria 17 (1996) 132–139. https://doi.org/10.1007/BF02665790.
[7] Q. Yang, C.G. Hu, S.X. Wang, Y. Xi, K.Y. Zhang, Tunable synthesis and thermoelectric property of Bi_2S_3 nanowires, J. Phys. Chem. C 117 (2013) 5515–5520. https://doi.org/10.1021/jp307742s.
[8] M.S. Silverman, High temperature, high pressure synthesis of a new bismuth sulfide, Inorg. Chem. 3 (7) (1964) 1041. https://doi.org/10.1021/ic50017a031.
[9] V.P.S. Awana, A. Kumar, R. Jha, S.K. Singh, A. Pal, Shriti, J. Saha, S. Patnaik, Appearance of superconductivity in layered $Lao_{0.5}F_{0.5}BiS_2$, Solid State Commun. 157 (2013) 21–23. https://doi.org/10.1016/j.ssc.2012.11.021.
[10] R. Jha, V.P.S. Awana, Superconductivity in layered $CeO_{0.5}F_{0.5}BiS_2$, J. Supercond. Nov. Magnetism 27 (2014) 1–4. https://doi.org/10.1007/s10948-013-2404-0.
[11] M. Nagao, A. Miura, S. Demura, K. Deguchi, S. Watauchi, T. Takei, Y. Takona, N. Kumada, I. Tananka, Growth and superconducting properties of F-substituted $ROBiS_2$ (R=La, Ce, Nd) single crystals, Solid State Commun. 178 (2014) 33–36. https://doi.org/10.1016/j.ssc.2013.10.019.
[12] J. Xing, S. Li, X.X. Ding, H. Yang, H.H. Wen, Superconductivity appears in the vicinity of semiconducting-like behavior in $CeO_{1-x}F_xBiS_2$, Phys. Rev. B 86 (2012) 21. https://doi.org/10.1103/PhysRevB.86.214518.
[13] Y. Mizuguchi, H. Fujihisa, Y. Gotoh, K. Suzuki, H. Usui, K. Kuroki, S. Demura, Y. Takano, H. Izawa, O. Miura, Novel BiS2-based layered superconductor $Bi_4O_4S_3$, Phys. Rev. B 86 (2012) 220510(R). https://doi.org/10.1103/PhysRevB.86.220510.
[14] M.R. Norman, High-temperature superconductivity in the iron pnictides, Physics 1 (2008) 21. https://doi.org/10.1103/Physics.1.21.
[15] Y. Mizuguchim, S. Demura, K. Deguchi, Y. Takano, Superconductivity in novel BiS_2-based layered superconductor $Lao_{1-x}F_xBiS_2$, J. Phys. Soc. Jpn. 81 (2012) 114725. https://doi.org/10.1143/JPSJ.81.114725.
[16] A. Omachi, J. Kajitani, T. Hiroi, O. Miura, Y. Mizuguchi, High-temperature thermoelectric properties of novel layered bismuth-sulfide $Lao_{1-x}F_xBiS_2$, J. Appl. Phys. 115 (2014), 083909. https://doi.org/10.1063/1.4867186.
[17] A. Yamamoto, D. Hashizume, M.S. Bahramy, Y. Tokura, Coexistence of monochalocogen and dichalocogen ions in $BiSe_2$ and BiS_2 crystals prepared at high pressure, Inorg. Chem. 54 (8) (2015) 4114–4119. https://doi.org/10.1021/acs.inorgchem.5b00349.
[18] K. Matsubayashi, T. Terai, J.S. Zhou, Y. Uwatoko, Superconductivity in the topological insulator Bi_2Te_3 under hydrostatic pressure, Phys. Rev. B 90 (2014) 125126. https://doi.org/10.1103/PhysRevB.90.125126.
[19] K.D. Leinenweber, J.A. Tyburczy, T.G. Sharp, E. Soignard, T. Diedrich, W.B. Petuskey, Y.B. Wang, J.L. Mosenfelder, Cell assemblies for reproducible multi-anvil experiments (the COMPRES assemblies), Am. Mineral. 97 (2012) 353–368. https://doi.org/10.2138/am.2012.3844.
[20] D. l. Decker, W.A. Bassett, t. Merrill, H.T. Hall, J.D. Barnett, High-pressure calibration - a critical review, J. Phys. Chem. Ref. Data 1 (1972) 3.
[21] K. Kato, H. Tanaka, Visualizing charge densities and electrostatic potentials in materials by synchrotron X-ray powder diffraction, Adv. Phys. X 1 (1) (2016) 55–80. https://doi.org/10.1080/23746149.2016.1142830.
[22] J. Rodríguez-Carvajal, Recent advances in magnetic structure determination by neutron powder diffraction, Physica B 192 (1993) 55–69. https://doi.org/10.1016/0921-4526(93)90108-I.
[23] M. Mezouar, W.A. Crichton, S. Bauchau, F. Thurel, H. Witsch, F. Torrecillas, G. Blattmann, P. Marion, Y. Dabin, J. Chavanne, O. Hignette, C. Morawe, C. Borel, Development of a new state-of-the-art beamline optimized for monochromatic single-crystal and powder X-ray diffraction under extreme conditions at the ESRF, J. Synchrotron Radiat. 12 (2005) 659–664. https://doi.org/10.1107/S0909049505023216.
[24] A. Dewaele, P. Loubeyre, M. Mezouar, Equations of state of six metals above 94 GPa, Phys. Rev. B 70 (9) (2004), 094112. https://doi.org/10.1103/PhysRevB.70.094112.
[25] L. Lutterotti, S. Matthies, H.R. Wenk, A.S. Schultz, J.W. Richardson, Texture and structure analysis of deformed limestone from neutron diffraction spectra, J. Appl. Phys. 81 (1997) 594–600. https://doi.org/10.1063/1.364220.
[26] L. Lutterotti, R. Vasin, H.R. Wenk, Rietveld texture analysis from synchrotron diffraction images. I. Calibration and basic analysis, Powder Diffr. 29 (1) (2014) 76–84. https://doi.org/10.1017/S0885715613001346.
[27] H.R. Wenk, L. Lutterotti, P. Kaercher, W. Kanitpanyacharoen, L. Miyagi, R. Vasin, Rietveld texture analysis from synchrotron diffraction images. II. Complex multiphase materials and diamond anvil cell experiments, Powder Diffr. 29 (3) (2014) 220–232. https://doi.org/10.1017/S0885715614000360.
[28] E. Antipov, E. Boldyreva, K. Friese, H. Huppertz, E. Tiekink, Z. Kristollogr. Cryst. Mater. 229 (5) (2014) 405–419.
[29] P. Giannozzi, S. Baroni, D. Ceresoli, et al., QUANTUM ESPRESSO: a modular and open-source software project for quantum simulations of materials, J. Phys. Condens. Matter 21 (2009) 395502. https://doi.org/10.1088/0953-8984/21/39/395502.
[30] N. Troullier, J.L. Martins, Efficient pseudopotentials for plane-wave calculations, Phys. Rev. B 43 (1993) 3. https://doi.org/10.1103/PhysRevB.43.1993.
[31] B.T.M. Willis, A.W. Pryor, Thermal Vibrations in Crystallography, Cambridge University Press, Cambridge, 1975.
[32] C.Y. Ho, R.W. Powell, P.E. Liley, Thermal conductivity of the elements: a comprehensive review, J. Phys. Chem. Ref. Data 3 (1) (1974) 1–796.
[33] I. Efthimiopoulos, J. Kemichick, X. Zhou, S.V. Khare, D. Ikuta, Y.J. Wang, High-pressure studies of Bi_2S_3, J. Phys. Chem. A 118 (2014) 1713–1720. https://doi.org/10.1021/jp4124666.
[34] L.F. Lundegaard, E. Makovicky, T. Boffa-Ballaran, T. Balic-Zunic, Crystal structure and cation lone electron pair activity of Bi_2S_3 between 0 and 10 GPa, Phys. Chem. Miner. 32 (2005) 578–584. https://doi.org/10.1007/s00269-005-0033-2.
[35] J.P. Perdew, K. Burke, M. Ernzerhof, Generalized gradient approximation made simple, Phys. Rev. Lett. 77 (18) (1996) 3865–3868. https://doi.org/10.1103/PhysRevLett.77.3865.
[36] J. Liu, D. Vanderbilt, Spin-orbit spillage as a measure of band inversion in insulators, Phys. Rev. B 90 (2014) 125133. https://doi.org/10.1103/PhysRevB.90.125133.
[37] M.Z. Hasan, C.L. Kane, Colloquium: topological insulators, Rev. Mod. Phys. 82 (4) (2010) 3045–3067. https://doi.org/10.1103/RevModPhys.82.3045.